PROGRESS IN PHOTOVOLTAICS: RESEARCH AND APPLICATIONS
Prog. Photovolt: Res. Appl. 2003; **11**:515–526 (DOI: 10.1002/pip.520)

Research

Quantitative Evaluation of Shunts in Solar Cells by Lock-In Thermography

O. Breitenstein*,†, J. P. Rakotoniaina and M. H. Al Rifai
Max Planck Institute of Microstructure Physics, Weinberg 2, D-06120 Halle, Germany

Infrared lock-in thermography allows to image shunts very sensitively in all kinds of solar cells and also to measure dark currents flowing in certain regions of the cell quantitatively. After a summary of the physical basis of lock-in thermography and its practical realization, four types of quantitative measurements are described: local I–V characteristics measured thermally up to a constant factor (LIVT); the quantitative measurement of the current through a local shunt; the evaluation of the influence of shunts on the efficiency of a cell as a function of the illumination intensity; and the mapping of the ideality factor n and the saturation current density J_0 over the whole cell. The investigation of a typical multicrystalline solar cell shows that the shunts are predominantly responsible for deterioration of the low-light-level performance of the cell, and that variations of the injection current density related to crystal defects are predominantly determined by variation of J_0 rather than of n. Copyright © 2003 John Wiley & Sons, Ltd.

KEY WORDS: shunts; thermography; lock-in; *I–V* characteristic; LIVT; efficiency; low light level performance

1. INTRODUCTION

Lock-in thermography has been established to be a reliable tool to locate shunts in all kinds of solar cells.[1–3] This technique is based on the application of a periodically pulsed bias voltage to the cell in the dark, and by measuring the surface temperature modulation by a sensitive infrared (IR) camera according to the lock-in principle. Since the phase of the T-modulation signal is not constant, two-channel lock-in detection has to be used. The lock-in correlation procedure consists in multiplying every information pixel of every incoming image in two logical channels by two different weighting factors, which change from image to image and may be positive or negative.[1] The results are added up in two separate frame-storages. In the first channel the weighting factors are approximating a sine function and in the other channel an inverse cosine function. Thus, after the measurement the image stored in the first frame-storage is proportional to the temperature modulation signal in-phase with the applied pulsed bias (0° signal; $T^0(x, y)$), and that in the other storage is proportional to the *T*-modulation signal phase-shifted against the bias pulses by −90° (−90° signal;

* Correspondence to: O. Breitenstein, Max Planck Institute of Microstructure Physics, Weinberg 2, D-06120 Halle, Germany.
†E-mail: breiten@mpi-halle.de
Contract/grant sponsor: BMWi; contract/grant number: 0329846 D (ASIS).
Contract/grant sponsor: EU; contract/grant number: ENK6-CT-2001-00573 (PORTRAIT).

Received 3 July 2003
Revised 5 September 2003

$T^{-90}(x, y)$). The $-90°$ signal is being used instead of the $+90°$ one since the latter is essentially negative. From these two images, the phase-independent amplitude (or magnitude) image $A(x, y)$ and the phase image $\Phi(x, y)$ can easily be calculated. In the positions of local shunts the amplitude image shows a bright contrast. More details about lock-in thermography can be found elsewhere.[1–3]

The aim of this paper is to show that lock-in thermography not only permits one to locate shunts, but also allows one to measure their current quantitatively. A presupposition for these quantitative measurements is that the investigated cell has a homogeneous IR emissivity. This can be secured most easily by covering the cell with a thin black-painted plastic film, held on to the cell by vacuum. This film serves as an efficient and homogeneous IR emitter.[1] After briefly describing the experimental technique of lock-in thermography in Section 2, the physical basis of quantitative investigations are summarized in Section 3. In Section 4 different types of measurement are desribed: the qualitative and quantitative measurement of the *I–V* characteristic of a local shunt; the evaluation of the influence of shunts on the efficiency of a cell as a function of the illumination intensity; and the mapping of the ideality factor n and the saturation current density J_0 over the whole cell. Some representative examples of such measurements are presented in Section 5.

2. EXPERIMENTAL

For all lock-in thermography investigations presented in Section 5 the TDL 384 M lock-in thermography system was used, which is commercially available from Thermosensorik GmbH Erlangen (Germany).[4] Contrary to other lock-in thermography systems[5,6] this system is specialized to the investigation of electronic components. With a resolution of 384 × 288 pixel and a sensitivity below 100 μK after 1000 s acquisition time it is the highest resolution and most sensitive system presently on the market. Figure 1 shows the functional scheme of this system. Instead of a complete universal IR camera it utilizes a special IR camera module, containing a Stirling-cooled mercury cadmium telluride (MCT) focal plane array (FPA) IR detector with 384 × 288 pixels, made by AIM Heilbronn.[7] The detector is sensitive in the 3–5 μm wavelength range and is read out with a full frame rate of about 120 Hz. If only part of the array is read out, the frame rate correspondingly increases up to 800 Hz for 128 × 128 pixel. This module also contains the logic read-out and digitizing units and the interface to a frame-grabber in the PC. By direct memory access (DMA) this frame-grabber writes the images cyclically in a certain RAM location of the PC, where they are picked up and evaluated by the lock-in software. A special hardware counter, which is synchronized to the camera module, generates the lock-in trigger signal, which pulses the power supply providing the sample bias. Additional to the lock-in processing, the PC also performs the digital image uniformity and missing pixel corrections, which in other systems are included in the IR camera itself.

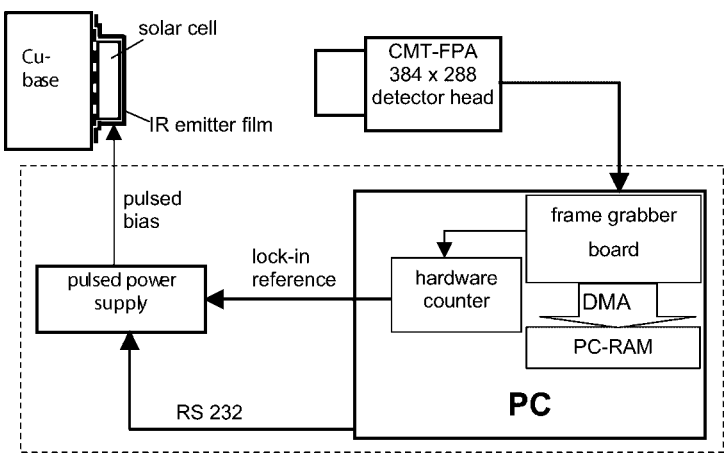

Figure 1. Functional scheme of the TDL 384 M lock-in thermography system[4]

3. PHYSICAL BASIS OF QUANTITATIVE LOCK-IN THERMOGRAPHY

The heat diffusion process underlying lock-in thermography is a linear process. Hence, the thermal waves coming from different heat sources are superimposed linearly. Moreover, if in any position the thermal signal is dominated by a well-defined heat source, the T-modulation amplitude in this position is proportional to the power of this heat source. If the lock-in frequency $f_{\text{lock-in}}$ is sufficiently high in the range of several Hz, and if the cell is not directly held by vacuum on a copper heat sink, but separated from it by a woven metal net providing a certain heat resistance layer,[1] it can be considered as adiabatic with respect to the lock-in frequency. Hence, the thermographic results are not influenced by any heat conduction to the surrounding. The linear superposition of thermal waves holds exactly only for each of the phase components $T^0(x,y)$ and $T^{-90}(x,y)$, but not for the amplitude (magnitude) signal $A(x,y)$, which is nonlinearly composed from $T^0(x,y)$ and $T^{-90}(x,y)$:

$$A(x,y) = \sqrt{(T^0(x,y))^2 + (T^{-90}(x,y))^2} \tag{1}$$

Note that for a point heat source the thermal signal at the source position is in-phase with the pulsed power and practically independent of the lock-in frequency, whereas that of an extended heat source is -90° phase-shifted and its amplitude drops with $1/f_{\text{lock-in}}$.[1] The distinction between localized and extended heat sources is given by the thermal diffusion length Λ, which drops with $1/\sqrt{f_{\text{lock-in}}}$ and is about 3 mm for silicon at $f_{\text{lock-in}} = 3$ Hz.[1] Hence, the signal-to-noise ratio of local and extended heat sources in the amplitude image depends on the lock-in frequency: For low frequencies extended heat sources become visible, but local heat sources appear blurred due to the lateral heat conduction, since the thermal diffusion length Λ is larger. For high frequencies, on the other hand, extended heat sources are increasingly embedded in noise, but local heat sources appear with a better effective spatial resolution.[1]

Owing to the linear superposition of thermal waves, the 0° and the -90° signals of an arbitrarily shaped local heat source can be thought to be composed of different point heat source contributions. So, to search for the optimum signal component for quantitatively evaluating lock-in thermograms, it is sufficient to consider the thermal waves around a point heat source, the radial distribution of which is shown in Figure 2 for a thermal diffusion length of $\Lambda = 3$ mm ($f_{\text{lock-in}} = 3$ Hz in Si). In the position of the source at $r = 0$ the 0° signal and the amplitude diverge, but the -90° signal remains finite. Of course, in reality the 0° signal also remains finite, since there is no real point heat source, and moreover the signal averages across at least one pixel of the IR camera. Note that the 0° signal shows a considerably stronger swing-over into the negative than the -90° signal for larger distances. Figure 3 shows the radial plane integral of the 0° and the -90° signal from the heat

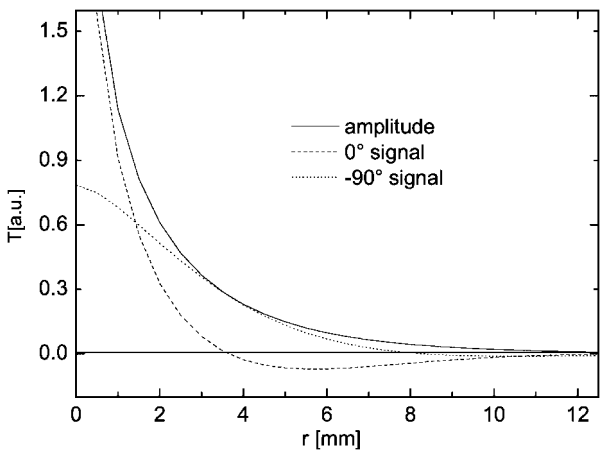

Figure 2. Radial distribution of the thermal signal around an oscillating point heat source: 0° signal, -90° signal, and amplitude signal

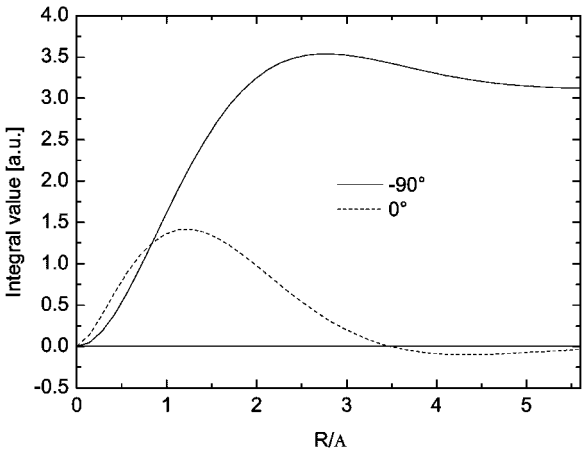

Figure 3. Radial plane integral of the 0° and the −90° signal around a point heat source as a function of the radius R (in units of the thermal diffusion lengh Λ)

source position up to an integration boundary distance R as a function of R. We see that for $R \to \infty$ the 0° signal converges to zero, whereas the −90° signal converges to a well-defined limiting value, which is proportional to the power of the source. Hence, the plane integral of the −90° signal of a local heat source is proportional to the source power, if the integration boundaries are chosen sufficiently distant from the source. In other words, within a sufficiently large area, the averaged 90° signal around a local shunt is proportional to the averaged dissipated power density in this area.

This also holds for a homogeneously heated region of any size, as well as for the whole solar cell area A_{cell}, where the dissipated power is known. This property, together with the general proportionality between the amplitude signal and the local power for a fixed lock-in frequency, is the physical basis of the quantitative evaluation of lock-in thermograms. Though all these considerations hold both for forward- and reverse-biasing the cell, we will concentrate here to forward-bias measurements, since we are mostly interested in the behaviour of shunts near the operation point of the cells.

4. QUANTITATIVE LOCK-IN THERMOGRAPHY INVESTIGATIONS

4.1 Local I–V characteristics measured thermally (LIVT)

If the thermal signal in the position of a local heat source (e.g., a shunt in a solar cell) is governed by this heat source, the amplitude of this signal is proportional to the dissipated power of this source. Hence, if the local bias is known, dividing the T-modulation amplitude signal $A(x, y)$ in the shunt position by the bias V yields the LIVT signal, which is proportional to the shunt current:[8]

$$\text{LIVT}(x, y) = \frac{A(x, y)}{V} \propto I(x, y) \tag{2}$$

By repeating this measurement for different applied biases, a local I–V characteristic can be measured thermally. As long as the shunts are not too strong and the cell is biased only into weak injection (below 0·6 V forward bias for sufficiently highly doped silicon solar cells), the externally applied bias V can usually be taken as the local bias in shunt position. If the series resistance to the shunt leads to a remarkable voltage drop, the local bias has to be measured independently by positioning a separate bias probe in shunt position. In principle, for a given solar cell and a given shunt geometry the thermal signal is uniquely connected with the dissipated power, hence the proportionality factor between the LIVT signal (in mK/V) and the shunt current is well defined. However, in reality a shunt may have a finite extension, which strongly affects this factor. Moreover, this factor is also dependent

on experimental parameters such as the real spatial resolution of the *T*-measurement, the lock-in frequency, the conversion factor of the IR camera, and on the IR emissivity, so that in reality the proportionality factor between LIVT and shunt current is often not exactly known. Nevertheless, in most cases the qualitative measurement of an *I–V* characteristic up to a constant factor gives valuable information about the current injection mechanism (e.g., linear or nonlinear characteristic, ideality factor). The following section describes how the LIVT signal can be scaled quantitatively without knowing any further experimental parameters.

4.2 *Quantitative measurement of shunt currents*

It has been mentioned in Section 3 that the average value of the -90° signal in a region around a shunt $\overline{T^{-90^\circ}_{\text{shunt}}}$ is proportional to the averaged dissipated heat in this region, having an area of A_{shunt}. This proportionality also holds for the signal averaged over the whole cell $\overline{T^{-90^\circ}_{\text{cell}}}$ having an area of A_{cell}, where we know the dissipated power to be the product of the applied bias V and the flowing cell current I_{cell}. Hence, from this measurement we can derive the unknown proportionality factor. If additionally to the shunt current a homogeneous current injection takes place leading to a homogeneous signal $\overline{T^{-90^\circ}_{\text{hom.}}}$, this signal can be subtracted from the shunt signal to obtain the net shunt current. These considerations finally lead to the following formula for the net shunt current:

$$I_{\text{shunt}} = \frac{I_{\text{cell}}\left(\overline{T^{-90^\circ}_{\text{shunt}}} - \overline{T^{-90^\circ}_{\text{hom}}}\right)}{\overline{T^{-90^\circ}_{\text{cell}}}} \frac{A_{\text{shunt}}}{A_{\text{cell}}} \tag{3}$$

This measurement can also be repeated for different biases, leading to a quantitative *I–V* characteristic for a single shunt, as one example in Section 5 will show. However, especially for low bias values the accuracy of this procedure is limited, since according to Figure 2 the -90° signal has a much lower magnitude in shunt position than the amplitude signal, which is used for the qualitative LIVT measurement. Therefore it is advisable to measure a local *I–V* characteristic first qualitatively according to Equation (2), using the amplitude signal and to scale it quantitatively by applying Equation (3) only for the largest bias, where the signal is highest and the experimental errors are lowest.

4.3 *Influence of shunts on the efficiency*

In many cases it is interesting to know how a certain group of shunts (e.g., all edge shunts), or how all local shunts in the cell influence the efficiency of the cell as a function of illumination intensity. This problem can be solved by applying the superposition principle, saying that the illuminated *I–V* characteristic is equal to the dark characteristic, shifted by the short circuit current I_{sc}. Here the effective series resistance of the cell R_{s} has to be regarded explicitely. Hence, first from the measured dark characteristic an R_{s}-corrected dark characteristic has to be calculated, this one has to be shifted by I_{sc} to obtain the illuminated characteristic without series resistance, and finally this has to be R_{s}-corrected. The series resistance R_{s} is chosen correctly if this illuminated characteristic, which was constructed from the dark one, comes close to the measured illuminated characteristic. If both characteristics do not converge, this may indicate spatial inhomogeneities of the series resistance in the given cell.

According to the considerations in Sections 3 and 4.2., the dark forward current in certain regions of the cell can be measured by averaging the -90° signal over these regions. For example, if the influence of the edge region of the cell has to be investigated, the signal $\overline{T^{-90^\circ}_{\text{no edge}}}$ can be measured in a region $A_{\text{no edge}}$, which is slightly smaller than the cell area, just excluding the regions where the thermal signal is influenced by the edge currents. Then a hypothetical dark current of the cell $I_{\text{no edge}}$ can be estimated, which would flow for a cell having the same area as the original one, but not being influenced by any edge currents:

$$I_{\text{no edge}} = I_{\text{cell}} \frac{\overline{T^{-90^\circ}_{\text{no edge}}}}{\overline{T^{-90^\circ}_{\text{cell}}}} \tag{4}$$

If the influence of all local shunts in the cell has to be evaluated, the value $\overline{T_{\text{hom}}^{-90^\circ}}$ measured in a region without any shunts leads to the current, which would be expected for a cell of the same area, which everywhere would show an *I–V* characteristic of the homogeneous region:

$$I_{\text{no shunts}} = I_{\text{cell}} \frac{\overline{T_{\text{hom}}^{-90^\circ}}}{\overline{T_{\text{cell}}^{-90^\circ}}} \tag{5}$$

Repeating the procedures of Equations (4) and (5) for different biases leads to hypothetical dark *I–V* characteristics with no edge shunts or with no shunts at all, which can be used to construct corresponding illuminated characteristics according to the procedure sketched above. Since the short-circuit current I_{sc} is proportional to the illumination intensity, these illuminated characteristics can be constructed for different values of the illumination intensity. From the maximum power point of these characteristics the efficiency of these hypothetical cells without shunts can be obtained, and the series resistance R_{s} fitted for the whole cell should be used. These results have to be compared with the real efficiency measured at the cell for different illumination intensities. From this comparison the influence of shunts on the efficiency can be concluded realistically, as the example in Section 5 will show.

4.4 Imaging the ideality factor and the saturation current density

It is usual to describe a non-exponential *I–V* characteristic formally by a bias-dependent ideality factor, which is equivalent to the piecewise approximation of the non-exponential characteristic by exponential segments:

$$J(V) = J_0(V)\exp\left(\frac{e\,V}{n(V)kT}\right) \tag{6}$$

where e = electron charge; V = forward-bias; kT = thermal energy; $n(V)$ = ideality factor; and $J_0(V)$ = saturation current density.

An ideal *pn* junction should show an ideality factor near unity over a large bias range, whereas in the positions of shunts, recombination sites, or other disturbations of the device, both J_0 and the ideality factor may be considerably larger. Note that to a first approximation (within the limit of the frequency-dependent spatial resolution of this technique) the lock-in thermography amplitude image $A(x, y)$ is proportional to the image of the local power density. Hence, if voltage drops at series resistances of a solar cell can be neglected, the quotient between the amplitude signal and the applied bias can be interpreted to be proportional to the two-dimensional distribution of the injection current density at the chosen bias (see the description of LIVT technique in Section 4.1.). So, if two lock-in thermograms $A^{V1}(x, y)$ and $A^{V2}(x, y)$ are taken at two different biases V_1 and V_2, the assumption of an exponential *I–V* characteristic of Equation (3) between V_1 and V_2 leads to the following formula for the local ideality factor between these two biases:[3]

$$n(x, y) = \frac{e(V_2 - V_1)}{kT \ln\left(\frac{A^{V_2}(x,y)V_1}{A^{V_1}(x,y)V_2}\right)} \tag{7}$$

The two biases V_1 and V_2 have to be chosen close to the operation point of the cell, but not so large that the series resistance plays a role. Appropriate values are $V_1 = 0{\cdot}5$ V and $V_2 = 0{\cdot}55$ V. For the saturation current density J_0 the following equation is obtained

$$J_0 = c^* \exp\left[\frac{V_2 \ln\left(\frac{A^{V1}(x,y)}{V_1}\right) - V_1 \ln\left(\frac{A^{V2}(x,y)}{V_2}\right)}{V_2 - V_1}\right]$$

with

$$c = \frac{I_2 V_2}{\overline{T^{V2}(x,y)} A_{\text{cell}}} \tag{8}$$

with I_2, V_2 and $\overline{A^{V2}(x,y)}$ being the current, the bias and the amplitude signal averaged over the whole cell of the second measurement. As the example in the following section will show, it is advantageous to display the image of the saturation current density on a logarithmic scale, since these values fluctuate over many orders of magnitude.

5. EXAMPLES OF QUANTITATIVE EVALUATIONS

The sample used for these investigations was a multicrystalline edge-defined film-fed growth (EFG) silicon solar cell 10×10 cm in size. All measurements have been carried out at a temperature of $25 \pm 0{\cdot}1$°C. Figure 4 shows an amplitude image of this cell measured at 3 Hz at a forward bias of 0·5 V with the different areas indicated, where the $-90°$ signal (which is not shown here) is averaged. Figure 5 shows the dark *I–V* characteristic of the upper point shunt in Figure 4 measured by the application of Equation (3) for all biases. This characteristic is highly nonlinear (exponential) with an ideality factor of about 6. This shunt lies below a grid line, so it is probably a Schottky-type shunt, where the grid metal is in contact with the base. Also all edge shunts show a nonlinear characteristic and are probably recombination induced. Figure 6 shows the measured dark *I–V* characteristic of the whole cell, the hypothetical characteristic of this cell without the edge shunts (but including the two point shunts) predicted by Equation (4), and that without any shunts, predicted by Equation (5). Figure 7 shows the efficiency in all these three cases, calculated from the dark characteristics of Figure 6, applying the superposition principle and correctly regarding the effective series resistance of this cell. In this case of nonlinear shunts the loss in efficiency due to the shunts is negligible at full illumination

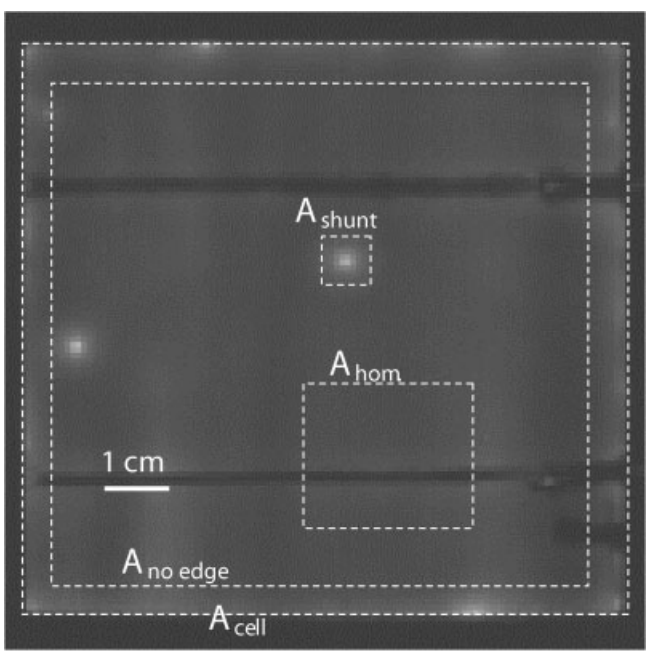

Figure 4. Lock-in thermogram (amplitude image, scaled to 2 mK) of a multicrystalline EFG solar cell measured at 0·5 V with different averaging areas indicated

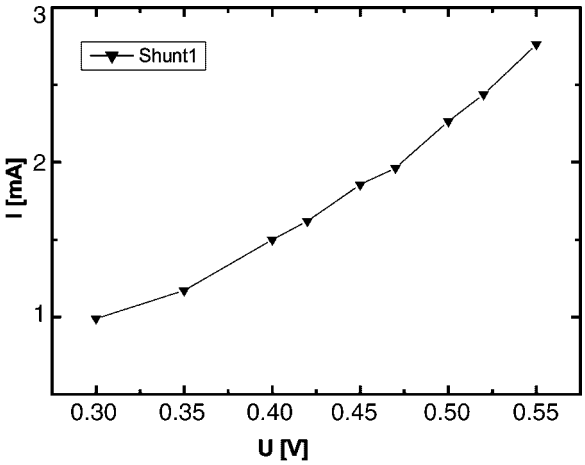

Figure 5. Thermally measured *I–V* characteristic of the local shunt framed in Figure 4

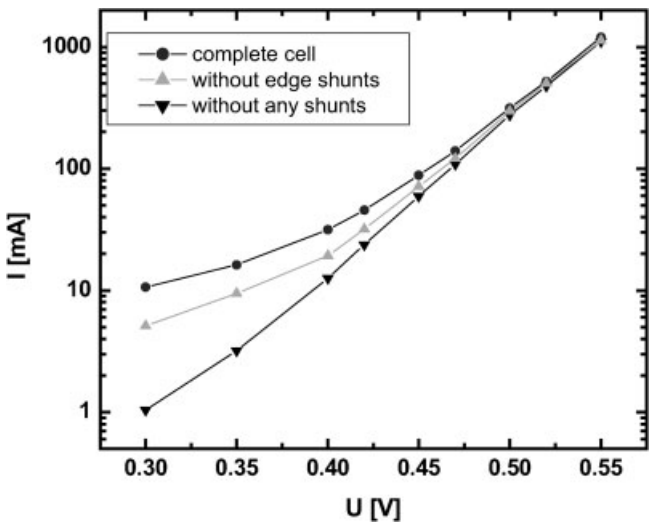

Figure 6. Measured dark *I–V* characteristic of the complete cell and simulated cells without edge shunts and without any shunts

intensity, and it is about 0·5% (absolute) at 100 W/m^2. However, in other cases of ohmic edge shunts we have shown[9] that these shunts may degrade the efficiency at 100 W/m^2 by about 2·5% (absolute).

Figure 8 shows a lock-in thermogram (amplitude image) measured at 0·55 V shown on the same scale as Figure 4, and Figure 9 shows a light-beam-induced current (LBIC) image of the investigated cell. There is a clear correlation between the thermogram and the LBIC signal; in the position of vertical dark stripes in the LBIC image there are bright stripes in the thermogram. This points to the fact that the dark forward current, which is reflected in the thermogram, is increased by the presence of recombinative crystal defects. Figure 10 shows the mapping of the ideality factor n according to Equation (7), and Figure 11 that of J_0 according to Equation (8), both based on the thermograms measured at 0·5 and at 0·55 V. All local shunts present a high n factor, above 5. This value agrees well with the n factor visible in the thermally measured local *I–V* characteristic of one of these shunts shown in Figure 5. Between 0·5 and 0·55 V, the n facor of the whole cell outside of the shunts is everywhere close to 1·4, whereas that of the measured characteristic (which is influenced by the shunts) is about 1·8.

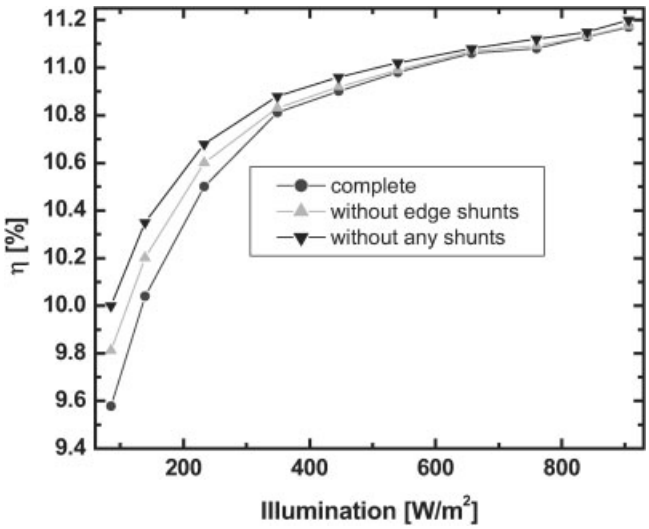

Figure 7. Measured efficiency of the cell and simulated efficiencies without edge shunts and without any shunts as a function of illumination intensity

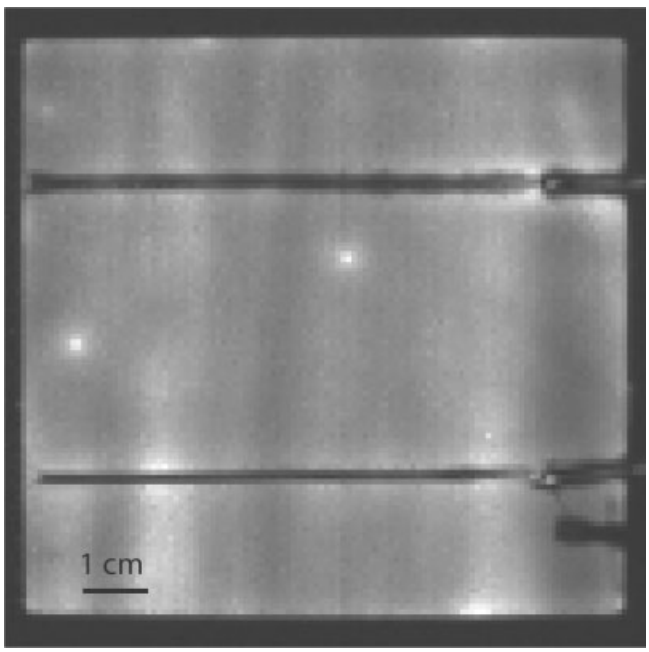

Figure 8. Lock-in thermogram (amplitude image, scaled to 2 mK) of the EFG solar cell measured at 0·55 V

The comparison between Figures 4 and 11 shows that local shunts present also regions of a high saturation current density, thus correlating with the n factor mapping results. However, the regions of poor crystal quality, which are easily visible in the LBIC image in Figure 9 and also in the thermogram in Figure 8, are weakly visible in the J_0 image (Figure 11, note the strongly expanded logarithmic scale), but not in the n factor image (Figure 10). This shows that the current injection mechanism in these regions differs qualitatively from that of local shunts. The nonlinear local shunts are mainly induced by local recombination currents, leading to a large n factor and an increased J_0. On the other hand, in the regions of poor crystal quality the diffusion current is larger, because a lower diffusion length in these regions is leading to an increased J_0, but the n factor remains low.

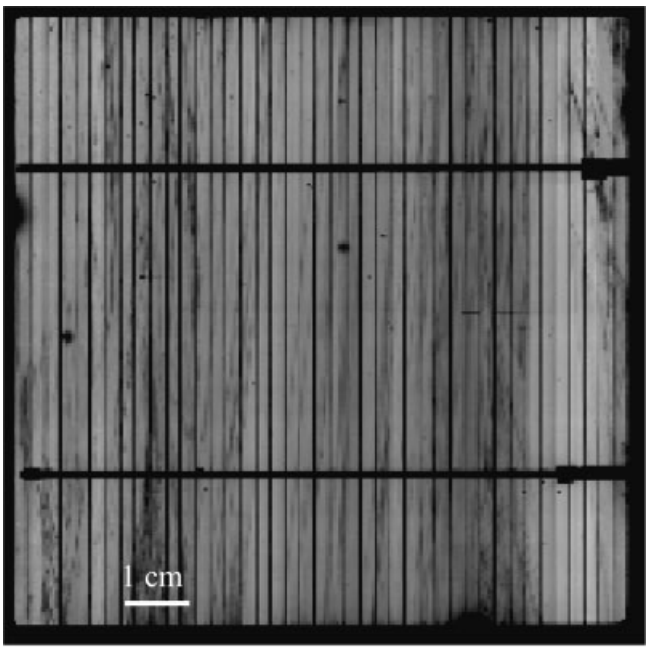

Figure 9. LBIC image of the investigated cell

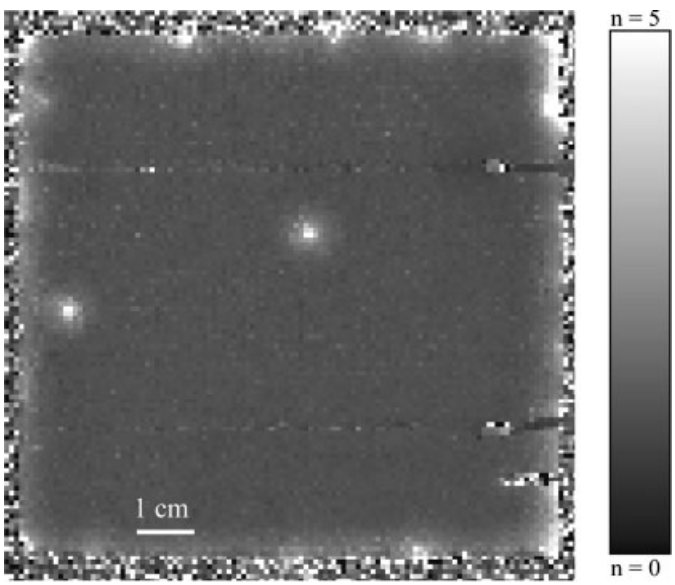

Figure 10. Ideality factor image according to Equation (6), measured between 0·5 and 0·55 V, scaled from $0 < n < 5$

6. CONCLUSIONS AND OUTLOOK

It has been shown that lock-in thermography allows one to perform a quantitative analysis of the spatial distribution of the dark forward current density of solar cells. Thus it is possible to measure thermally the *I–V* characteristic of point shunts in a non-destructive way. The accuracy of this method was demonstrated[10] by comparison with local emitter potential mapping (PRAMP). In fact, both independent measurements lead to

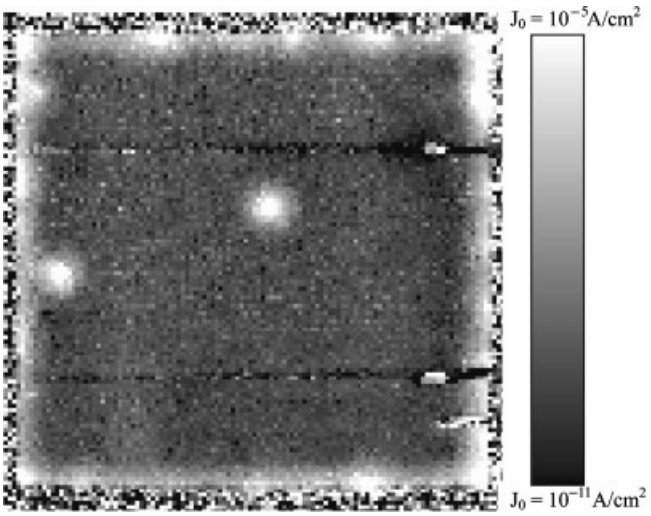

Figure 11. Saturation current density image according to Equation (6), measured between 0·5 and 0·55 V, logarithmically scaled from $10^{-11} < J_0 < 10^{-5}$ A/cm^2

the same current values within an accuracy of 10% (A.S.H. van der Heide, ECN Petten, personal communication). As another type of quantitative analysis of lock-in thermograms, a hypothetical solar cell without any shunts can be modelled, whereby the influence of shunts on the efficiency as a function of the illumination intensity can be estimated. Finally, the mapping of the ideality factor n and of the saturation current density J_0 allows one to draw conclusions as to the current injection mechanism in different regions of the cell. Note that all these investigations can also be carried out at different sample temperatures. This allows a further physical characterization of shunts with respect to their temperature dependence, thereby enabling a mapping of the activation energy of thermally activated currents.[11]

The quantitative investigation on a multicrystalline solar cell showed that all local shunts in this cell show a nonlinear (exponential) *I–V* characteristic with an ideality factor above 5, but the whole undisturbed cell area shows an ideality factor close to 1·4. In fact, all our previous investigations point to the fact that in multicrystalline solar cells the dominant 'second diode current' can be attributed to nonlinear local shunts and is not due to homogeneously distributed point defect recombination in the space charge layer, as often assumed.[3,9]

As discussed in Section 3, the effective spatial resolution of all techniques described here is influenced by lateral heat diffusion and determined by the frequency-dependent thermal diffusion length Λ, which cannot be chosen arbitrarily small. Therefore, e.g., in the ideality factor and saturation current images the local shunts are surrounded by a distinct halo, which has to be considered as a heat-diffusion-induced artifact. Only the signal values in shunt position display the parameters of the shunt. However, if the signal-to-noise ratio of a lock-in thermogram is sufficiently large, mathematical spatial deconvolution is an option to get rid of the lateral thermal diffusion effects and to convert a lock-in thermogram directly into a lateral power distribution.[12] This is another kind of quantitative evaluation of thermographic results, which has the advantage of yielding an improved spatial resolution. This improvement, however, comes at the expense of a degradation of the signal-to-noise ratio, which is inherent to all spatial deconvolution procedures.[12]

Note finally that IR thermography is a fairly universal tool, which is not restricted to shunt investigations in solar cell research and industry. Lock-in thermography can also be used, e.g., for the fast mapping of the minority carrier lifetime in semiconductor wafers by using the carrier density imaging technique[13] (CDI), which is based on the work of Bail *et al.*[14] Moreover, infrared imaging can be used to investigate hot spots under reverse bias, which may become detrimental if a module is partly shaded, as well as for detecting faults in complete solar modules.[15] This universal applicability of an infrared camera may be an argument for using this technique in spite of its considerable expense.

Acknowledgements

The authors are indebted to M. Langenkamp (Rendsburg), I. Konovalov (Leipzig), and A.S.H. van der Heide (ECN Petten) for experimental cooperation, and to RWE Schott Solar GmbH for supplying the EFG solar cell used for this investigation. This work was supported by project BMWi 0329846 D (ASIS) and by EU project ENK6-CT-2001-00573 (PORTRAIT). This paper is an extended version of a contribution to the 3rd World Conference on Photovoltaic Energy Conversion, held 11–18 May 2003 in Osaka, Japan.

REFERENCES

1. Breitenstein O, Langenkamp M. *Lock-in Thermography—Basics and Application to Functional Diagnostics of Electronic Components*. *Advanced Microelectronics Volume 10*. Springer: Heidelberg, Berlin; 2003.
2. Breitenstein O, Langenkamp M, Lang O, Schirrmacher A. Shunts due to laser scribing of solar cells evaluated by highly sensitive lock-in thermography. *Solar Energy Materials and Solar Cells* 2001; **65**: 55–62.
3. Breitenstein O, Langenkamp M, Rakotoniaina JP, Zettner J. The imaging of shunts by infrared lock-in thermography. *Proceedings of the 17th European Photovoltaic Solar Energy Conference*, Munich, 2002; 1499–1502.
4. www.thermosensorik.de
5. www.cedip-infrared.com
6. www.stressphotonics.com
7. www.aim-ir.de
8. Konovalov IE, Breitenstein O, Iwig K. Local current–voltage curves measured thermally (LIVT): a new technique of characterizing PV cells. *Solar Energy Materials and Solar Cells* 1997; **48**: 53–60.
9. Breitenstein O, Langenkamp M. Quantitative local analysis of *I–V* characteristics of solar cells by thermal methods. *Proceedings of the 2nd World Conference on Photovoltaic Solar Energy Conversion*, Vienna, 1998; 1382–1385.
10. van der Heide ASH, Bultman JH, Hoornstra J, Schönecker A. Contact resistances measured using the corescan: relations with cell processing. *Proceedings of the 2nd World Conference on Photovoltaic Solar Energy Conversion*, Vienna, 1998; 1531–1534.
11. Konovalov I, Strikha V, Breitenstein O. Activation energy of local currents in solar cells measured by thermal methods. *Progress in Photovoltaics: Research and Applications* 1998; **6**: 151–161.
12. Breitenstein O, Konovalov I, Langenkamp M. Highly sensitive lock-in thermography of local heat sources using 2-dimensional spatial deconvolution. *Proceedings of Quantitative Infrared Thermography 5*, Reims, 2000; 218–223.
13. Isenberg J, Riepe S, Glunz SW, Warta W. Carrier density imaging (CDI): a spatially resolved lifetime measurement suitable for in-line process-control. *Proceedings of the 29th IEEE Photovoltaic Specialists Conference*, New Orleans, 2002; 266–269.
14. Bail M, Kentsch J, Brendel R, Schulz M. Lifetime mapping of Si wafers by an infrared camera. *Proceedings of the 28th IEEE Photovoltaic Specialists Conference*, Anchorage, 2000; 99–103.
15. King DL, Kratochvil JA, Quintana MA. Applications for infrared imaging equipment in photovoltaic cell, module, and system testing. *Proceedings of the 28th IEEE Photovoltaic Specialists Conference*, Anchorage, 2000; 1487–1490.

